RAA 2017 Vol. **17** No. **8**, 87 (14pp) doi: 10.1088/1674–4527/17/8/87

http://www.raa-journal.org *http://iopscience.iop.org/raa*

***R**esearch in*
***A**stronomy and*
***A**strophysics*

Physical properties and catalog of EW-type eclipsing binaries observed by LAMOST

Sheng-Bang Qian[1,2,3,4], Jia-Jia He[1,2,3], Jia Zhang[1,2,3], Li-Ying Zhu[1,2,3,4], Xiang-Dong Shi[1,2,3], Er-Gang Zhao[1,2,3,4] and Xiao Zhou[1,2,3]

[1] Yunnan Observatories, Chinese Academy of Sciences, Kunming 650011, China; *qsb@ynao.ac.cn*
[2] Key Laboratory of the Structure and Evolution of Celestial Objects, Chinese Academy of Sciences, Kunming 650216, China
[3] Center for Astronomical Mega-Science, Chinese Academy of Sciences, Beijing 100012, China
[4] University of the Chinese Academy of Sciences, Beijing 100049, China

Received 2017 March 31; accepted 2017 May 8

Abstract EW-type eclipsing binaries (hereafter called EWs) are strong interacting systems in which both component stars usually fill their critical Roche lobes and share a common envelope. Numerous EWs were discovered by several deep photometric surveys and there were about 40 785 EW-type binary systems listed in the international variable star index (VSX) by 2017 March 13. 7938 of them were observed with LAMOST by 2016 November 30 and their spectral types were identified. Stellar atmospheric parameters of 5363 EW-type binary stars were determined based on good spectroscopic observations. In the paper, those EWs are cataloged and their properties are analyzed. The distributions of orbital period (P), effective temperature (T), gravitational acceleration ($\log(g)$), metallicity ([Fe/H]) and radial velocity (RV) are presented for these observed EW-type systems. It is shown that about 80.6% of sample stars have metallicity below zero, indicating that EW-type systems are old stellar populations. This is in agreement with the conclusion that EW binaries are formed from moderately close binaries through angular momentum loss via magnetic braking that takes a few hundred million to a few billion years. The unusually high metallicities of a few percent of EWs may be caused by contamination of material from the evolution of unseen neutron stars or black holes in the systems. The correlations between orbital period and effective temperature, gravitational acceleration and metallicity are presented and their scatters are mainly caused by (i) the presence of third bodies and (ii) sometimes wrongly determined periods. It is shown that some EWs contain evolved component stars and the physical properties of EWs mainly depend on their orbital periods. It is found that extremely short-period EWs may be older than their long-period cousins because they have lower metallicities. This reveals that they have a longer timescale of pre-contact evolution and their formation and evolution are mainly driven by angular momentum loss via magnetic braking.

Key words: stars: binaries: close — stars: binaries: spectroscopic — stars: binaries: eclipsing — stars: evolution

1 INTRODUCTION

EW-type eclipsing binaries (hereafter called EWs) usually consist of two ellipsoidal FGK dwarfs that are in contact with each other and share a common convective envelope (CCE) that is lying between the inner and outer critical Roche-lobe surfaces. They are W Ursae Majoris-type eclipsing variables with periods shorter than one day. Their light variation is continuous and it is impossible to specify the exact times of onset and end of eclipses. Their light amplitudes are usually < 0.8 mag in V and the depths of the primary and secondary minima are al-

most equal (e.g., Samus et al. 2017). This indicates that the two components possess almost identical temperature and are in thermal contact in spite of different component masses. This kind of star system is different from EB-type binaries whose depths of primary and secondary minima are not equal and they are not in thermal contact. EW-type binaries are usually detected in older open clusters and globular clusters (e.g., Kaluzny & Rucinski 1993), but they are absent in young stellar clusters (e.g., Rucinski 1998). Based on these observational facts, some investigators assumed that EW-type binaries form from short-period detached binaries through angular momentum loss via magnetic braking (e.g., Guinan & Bradstreet 1988; Bradstreet & Guinan 1994) and will merge into rapidly rotating single stars (e. g., Zhu et al. 2016). The timescale of pre-contact evolution is from a few hundred million to a few billion years. However, how EW binaries form is still unknown. It is possible that third bodies may play an important role in the origin of EWs by removing angular momentum from the central binary through early dynamical interaction and/or later evolution (e.g. Qian et al. 2014, Zhu et al. 2013a).

Thanks to several photometric surveys, such as the Catalina Sky Survey[1] (CSS, Drake et al. 2009, 2014), the asteroid survey LINEAR[2] (Palaversa et al. 2013), All Sky Automated Survey[3] (ASAS, Pojmanski 1997; Pojmanski et al. 2005) and Northern Sky Variability Survey[4] (NSVS, Woźniak et al. 2004), a large number of EW binaries have been discovered. Since the data on variable stars including EWs are constantly being updated, the mission of VSX[5] (the international variable star index, Watson 2006) is to compile all of the new information together in a single data repository and provide tools necessary for the controlled and secure revision of the data. 40 785 EW-type binary systems were listed in VSX by 2017 March 13. Among the 40 785 EWs, the orbital periods of 40 646 systems were included. Those survey data are very useful for understanding the photometric properties of EW binaries. However, statistical spectroscopic properties of those sample stars are unclear because of the lack of spectral surveys. The light curves of many EW binaries have been observed recently, but their spectral types are generally unknown.

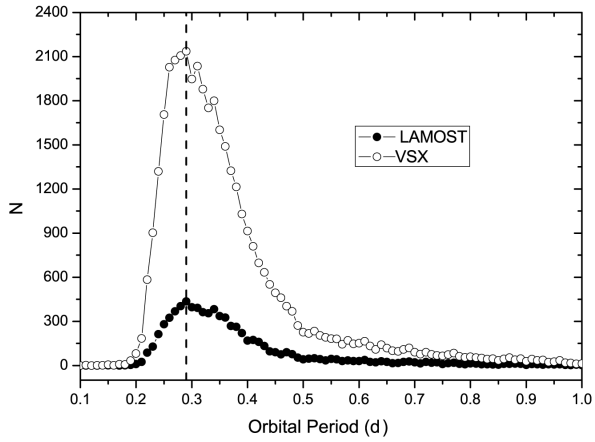

Fig. 1 Period distribution of EWs. Open circles represent systems listed in the VSX catalog, while solid dots signify binaries observed by LAMOST. The peaks of the two period distributions are near 0.29 d (the dashed line).

The Large Sky Area Multi-Object Fiber Spectroscopic Telescope (LAMOST, also called the Guo Shou Jing Telescope) is a special telescope with an effective aperture of about 4 meters that is located at Xinglong Station, administered by National Astronomical Observatories, Chinese Academy of Sciences. It has a field of view of 5 degrees and can simultaneously obtain the spectra of about 4000 stars with low-resolution of about 1800 in one exposure (Wang et al. 1996; Cui et al. 2012). The wavelength range of LAMOST is from 3700 to 9000 Å and is divided into two arms, i.e., a blue arm (3700–5900 Å) and a red arm (5700–9000 Å). The final spectrum of each target is obtained by merging several exposures. Huge amounts of spectroscopic data have been obtained (e.g., Zhao et al. 2012; Luo et al. 2012, 2015).

In recent LAMOST data releases, about 19.5% of EW-type binaries (7938) in VSX were observed by the LAMOST survey from 2011 October 24 to 2016 November 30. Among the 7938 EWs, the orbital periods of 7930 samples are included in VSX. The distribution of the orbital period for EWs observed by LAMOST is shown in Figure 1. Also displayed in the figure is the period distribution of all EWs in VSX, in which 139 EWs without orbital periods are not shown. Those spectroscopic data can be used during the photometric solutions and the large amount of data representing stellar spectra from the LAMOST survey provide important information for studying EWs. In the paper, EW binaries observed in the LAMOST survey are cataloged. Then, based on the distributions of those atmospheric parame-

[1] *http://www.lpl.arizona.edu/css/*
[2] *https://astroweb.lanl.gov/lineardb/*
[3] *http://www.astrouw.edu.pl/asas/*
[4] *http://www.skydot.lanl.gov/nsvs/nsvs.php*
[5] *http://www.aavso.org/vsx/*

ters and some statistical correlations, the physical properties and the formation and evolutionary states of EW binaries are discussed.

2 CATALOG OF EWS OBSERVED BY LAMOST

In recent LAMOST data releases, about 7938 EWs in the VSX catalog were observed from 2011 October 24 to 2016 November 30 and their spectral types were obtained. Among the 7938 EWs, the stellar atmospheric parameters of 5363 systems were determined when their spectra had sufficiently high signal to noise. The stellar atmospheric parameters including the effective temperature $T_{\rm eff}$, gravitational acceleration $\log(g)$, metallicity [Fe/H] and radial velocity (RV) $V_{\rm r}$ were automatically derived by the LAMOST stellar parameter pipeline when their spectra were of high quality (Wu et al. 2011b, 2014; Luo et al. 2015). Those stellar atmospheric parameters were determined based on the Universite de Lyon spectroscopic analysis software (ULySS) (Koleva et al. 2009; Wu et al. 2011a). ULySS fits complete observed spectra by using a model spectrum that is generated by an interpolator by using the ELODIE library as a reference (e.g., Prugniel & Soubiran 2001; Prugniel et al. 2007). When $T_{\rm eff} < 8000$ K, the standard deviations are 110 K, 0.19 dex and 0.11 dex for $T_{\rm eff}$, $\log(g)$ and [Fe/H] respectively. For RV $V_{\rm r}$, the standard deviations are 4.91 km s^{-1} when $T_{\rm eff} < 10\,000$ K (e.g., Gao et al. 2015).

The observations of 5363 EWs are cataloged in order of increasing VSX number. Some EWs were observed twice or more on different dates and we list all of the parameters. Values listed in Table 1 are the first 20 observations. The whole catalog is available through the internet (the electronic version of the catalog is at the website[6]) and it will be improved by adding new data obtained by LAMOST in the future. The table includes names of the binaries, their right ascension (R.A.) and declination (Dec.) coordinates, types of light variation and orbital periods. These parameters are from the VSX catalog. Entries shown in Column (6) are the distances (in arcsec) between the two positions determined by the coordinates given in VSX and by LAMOST. These distances were used to identify EWs from the LAMOST samples based on the criterion Dist$< 2''$. The observing dates are listed in Column (7), while the determined spectral types of EWs are shown in Column (8). The stellar atmospheric parameters $T_{\rm eff}$, $\log(g)$, [Fe/H] and $V_{\rm r}$ of the 5363 EWs are listed in Columns (9), (11), (13) and (15) respectively, and E_1, E_2, E_3 and E_4 in the table are their corresponding errors.

The temperatures of most EWs are lower than 8000 K and their standard deviations could be estimated reliably. However, both components of EWs are rapidly rotating and highly deformed stars that share a common envelope. Do their spectra have sufficient tracers necessary for unique determination of atmospheric parameters? There are 25 EWs that were observed five times or more. To check the reliability of stellar atmospheric parameters and to answer the question, we determined the mean values of their atmospheric parameters and derived the corresponding standard errors.

The results are shown in Table 2 where their names and orbital periods are listed in the first and second columns respectively. The observational times are shown in the third column, while the average atmospheric parameters and their standard errors are displayed in the other columns. As shown in Table 2, standard errors of the effective temperatures for all targets are lower than 110 K. Apart from two targets, the standard errors of the gravitational acceleration $\log(g)$ for the other targets are lower than 0.19 dex. The standard errors of the metallicity for most EW targets are lower than 0.11 dex. These results may indicate that it does no matter if we use single star spectra to calibrate peanut-shaped stars and demonstrate that the extracted parameters could reach the mentioned level of precision. Moreover, because those EWs were observed at different phases, the associated results also reveal that there are no obvious effects of phase on the derived atmospheric parameters across multiple observations of the same object within errors.

The relative distribution (the percentage of the number to the whole sample) of orbital period for the 5363 EWs is displayed in Figure 2. For comparison, the relative period distribution of all EWs in VSX is also shown in the figure. It is found that they nearly overlap. This indicates that the 5363 EWs could be used to represent the properties of all EWs in the complete VSX catalog. As shown in Figures 1 and 2, the period distribution peaks are near 0.29 d (dashed line). This is shorter than that given by Paczyński et al. (2006) who obtain a peak near 0.37 d based on ASAS data (e.g., Pojmanski 1997; Pojmanski et al. 2005). This may be caused by the fact that ASAS is dedicated to the detection of variability in bright stars, but many faint short-period EWs were discovered by recent deep photometric surveys (e.g., Drake et al. 2009, 2014). Like cases analyzed by several investigators (e.g., Paczyński et al. 2006; Becker et al. 2011),

[6] *http://search.vbscn.com/CEW.table1.txt*

Table 1 Catalog of EWs Observed by LAMOST (the first 20 observations)

Name	R.A.	Dec.	Type	P (d)	Dist	Date	Sp.	T (K)	E_1	$\log(g)$	E_2	[Fe/H]	E_3	$V_{\rm r}$ (km s^{-1})	E_4
(1)	(2)	(3)	(4)	(5)	(6)	(7)	(8)	(9)	(10)	(11)	(12)	(13)	(14)	(15)	(16)
HU And	003929.69	+400459.8	EW	0.285789	0.360	2011–10–28	G9	5158.97	246.09	4.431	0.352	0.126	0.229	0.73	18.92
IM And	004646.80	+393833.0	EW	0.270377	1.108	2014–12–12	K3	4764.13	208.42	4.182	0.299	–0.143	0.194	–136.85	15.35
IM And	004646.80	+393833.0	EW	0.270377	1.108	2015–09–13	K5	4977.45	73.29	4.692	0.105	–0.029	0.068	–157.15	5.28
LY And	022152.54	+383742.4	EW	0.34505	0.613	2013–11–12	G2	5751.81	29.16	4.090	0.041	–0.315	0.027	0.16	2.75
MT And	022704.78	+400328.5	EW	0.358781	0.767	2013–11–12	G3	5676.33	204.28	3.931	0.293	–0.136	0.190	14.41	15.32
MT And	022704.78	+400328.5	EW	0.358781	0.911	2013–10–14	G3	5751.14	25.60	4.144	0.035	0.005	0.024	–17.61	2.62
QX And	015757.78	+374822.5	EW	0.4121753	0.045	2014–11–10	F5	6501.66	2.24	4.174	0.001	–0.066	0.002	4.53	0.49
GK Aqr	221956.93	–007986.9	EW	0.3274145	0.344	2016–11–03	K0	5302.35	7.27	4.274	0.005	0.384	0.006	–17.35	1.81
GK Aqr	221956.93	–007986.9	EW	0.3274145	1.188	2012–10–04	K1	5365.27	56.54	4.368	0.080	0.458	0.053	–55.10	5.00
GM Aqr	222157.94	–028042.8	EW	0.3672853	0.491	2016–11–03	G7	5636.36	21.72	4.296	0.030	0.153	0.021	–66.66	2.33
GM Aqr	222157.94	–028042.8	EW	0.3672853	0.491	2012–10–04	G7	5715.99	132.99	4.308	0.190	0.109	0.124	34.44	10.36
GS Aqr	222733.63	–005757.6	EW	0.374067	1.671	2015–11–09	A5V	7023.10	3.25	4.276	0.002	–1.038	0.003	–53.16	0.81
GS Aqr	222733.63	–005757.6	EW	0.374067	0.479	2016–11–03	A7V	7027.32	7.89	4.323	0.010	–0.938	0.008	–112.34	1.25
AH Aur	062604.93	+275956.4	EW/KW	0.494106	0.267	2012–02–01	G3	6017.81	14.79	4.025	0.020	0.399	0.014	48.62	1.68
V0468 Aur	045611.66	+444638.9	EW	0.91278951	0.050	2012–02–09	F5	6548.18	182.53	3.856	0.262	–0.001	0.170	13.64	13.48
TU Boo	140458.04	+300001.5	EW/KW	0.3242868	0.144	2014–03–25	G3	5828.78	9.41	4.295	0.012	–0.027	0.009	7.13	1.32
TU Boo	140458.04	+300001.5	EW/KW	0.3242868	0.144	2016–05–18	G3	5710.93	9.32	4.165	0.012	–0.095	0.009	–13.39	1.24
TZ Boo	150809.13	+395812.9	EW/KW	0.297162	0.081	2016–02–25	G2	5597.28	6.21	4.179	0.008	–0.746	0.006	–59.65	0.92
AK Boo	133839.06	+241105.4	EW/KE	0.694030	0.436	2015–03–19	G7	5526.82	95.45	4.065	0.136	–0.326	0.089	45.21	7.77
AQ Boo	134726.86	+171824.7	EW	0.333139	0.936	2014–03–06	G0	5680.80	2.64	4.037	0.002	–0.466	0.002	–52.13	0.59

Table 2 Mean Atmospheric Parameters for 25 EWs Observed More than Four Times and Their Standard Errors

Star name	P (d)	Times	$\overline{T_{\rm eff}}$ (K)	Errors	$\overline{\log(g)}$	Errors	$\overline{[{\rm Fe/H}]}$	Errors
T-Lyr1-15705	0.298933	8	5473.44	68.40	4.340	0.101	0.117	0.070
LINEAR 6102187	0.324026	7	5479.31	94.55	4.234	0.153	–0.047	0.041
CSS J074328.7+360725	0.391234	6	6158.67	67.58	4.157	0.072	–0.084	0.123
CSS J222851.7+065242	0.370323	5	6687.61	109.41	4.064	0.104	–0.322	0.089
CSS J111218.6+542629	0.317854	5	5421.22	61.99	4.339	0.072	–0.042	0.031
CSS J093510.3+313745	0.295414	5	6056.15	72.54	4.089	0.090	–0.572	0.017
CSS J090411.9+132908	0.273486	5	5135.15	33.33	4.165	0.090	–0.404	0.058
CSS J082217.4+064452	0.340438	5	5780.39	89.51	4.070	0.192	–0.236	0.093
CSS J073220.4+283612	0.274257	5	5330.87	47.72	4.332	0.113	–0.189	0.041
CSS J070315.8+423814	0.368082	5	5767.00	62.65	4.173	0.080	0.099	0.041
CSS J025901.9+313046	1.0544407	5	6304.31	46.60	3.754	0.091	0.148	0.068
CSS J025613.4+311517	0.538159	5	6237.42	46.37	4.106	0.020	–0.083	0.034
CSS J022913.6+042841	0.29825	5	5838.94	48.30	4.187	0.166	–0.755	0.189
CSS J011822.4+080543	0.454696	5	6119.61	56.82	4.131	0.124	–0.557	0.017
CSS J011310.1+370333	0.39251	5	6077.21	65.25	4.123	0.055	–0.177	0.051
LINEAR 6446092	0.30679788	5	5484.59	43.30	4.381	0.196	0.172	0.068
NSVS 4831297	0.369811	5	5926.45	24.09	4.202	0.086	0.202	0.053
KID 06964796	0.399961	5	5939.73	27.60	4.237	0.044	0.133	0.014
KID 11084782	0.586555	5	8222.08	17.16	4.011	0.018	–0.269	0.025
NSVS 4583537	0.40835410	5	6284.33	66.72	4.120	0.042	–0.111	0.049
VSX J065147.6+592649	0.4217	5	5996.10	35.18	4.127	0.079	0.411	0.018
NY Boo	0.32679	5	5779.52	30.98	4.115	0.055	–0.076	0.027
NSVS 7209962	0.295931	5	5276.37	37.39	4.273	0.080	0.348	0.055
OP Leo	0.391931	5	6104.86	51.49	4.129	0.061	–0.385	0.053
ASAS J081149–0111.1	0.567286	5	6275.02	93.33	4.346	0.030	0.143	0.034
V0449 Gem	0.270659	5	5045.36	42.53	4.321	0.049	–0.048	0.026
V1022 Tau	0.34717194	5	5882.69	52.00	4.193	0.049	–0.255	0.045

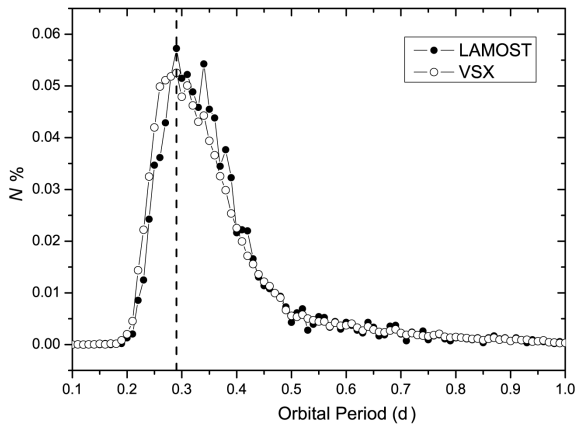

Fig. 2 Relative distribution of orbital period for EWs. Open circles refer to all EWs listed in the VSX catalog, while solid dots are those 5363 EWs whose stellar atmospheric parameters were determined by using LAMOST data. The period distribution peaks are near 0.29 d (dashed line).

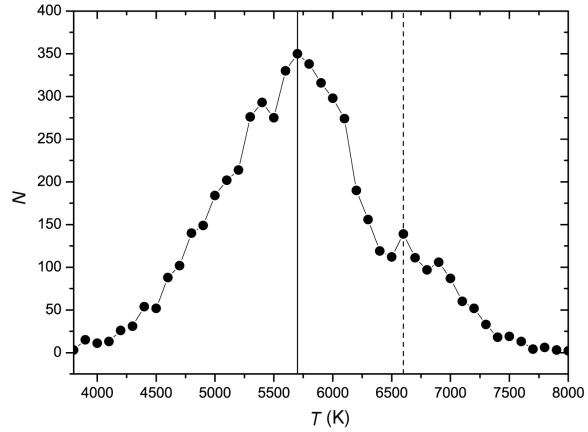

Fig. 3 Distribution of the effective temperature for EWs observed by LAMOST. Solid and dashed lines refer to the two peaks near 5700 K and 6600 K respectively.

it has a sharp cut-off at 0.2 d. A long tail exceeds 1 d and the tail actually extends to about 24 d.

For some LAMOST spectra of EW-type binaries, their signal to noise values are not high enough to determine the stellar atmospheric parameters. In those cases, only spectral types were identified. The spectral types of those EWs are also cataloged in order of increasing VSX number. The entries shown in Table 3 are the first 20 spectral types in the catalog. The whole table is available at the website[7] via the internet. The catalog lists 3732 spectral types for 3055 EWs. Descriptions for those columns are the same as those in Table 1. For about 1691

[7] *http://search.vbscn.com/CEW.table3.txt*

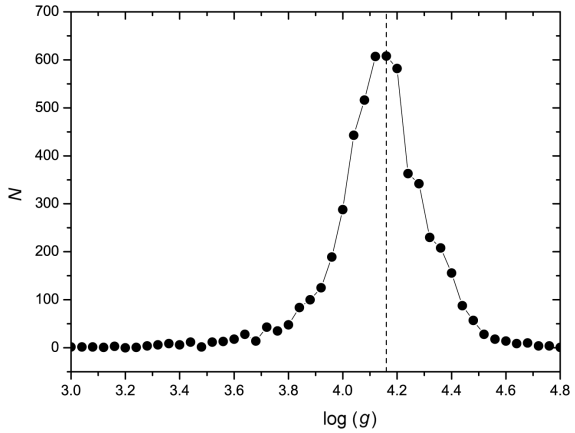

Fig. 4 Distribution of gravitational acceleration $\log(g)$ for EWs observed by LAMOST. The dashed line refers to the peak near 4.16.

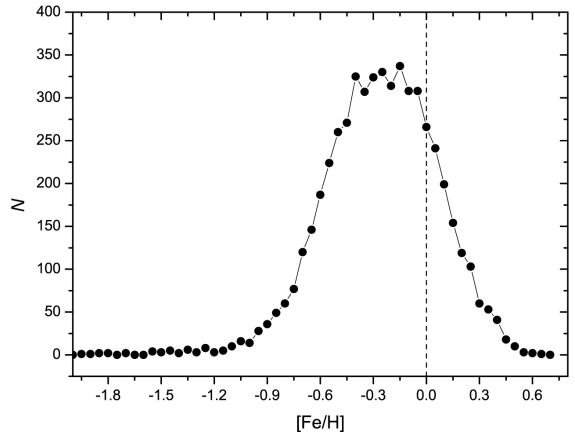

Fig. 5 Distribution of metallicity [Fe/H] for EWs observed by LAMOST. It is apparent that most of the EWs have [Fe/H]< 0.

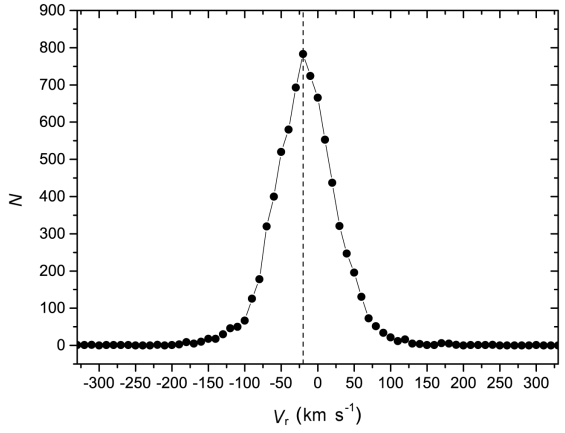

Fig. 6 Distribution of RV $V_{\rm r}$ for EWs observed by LAMOST. There is a peak near $V_{\rm r} = -20\,{\rm km\,s^{-1}}$.

EWs, only the spectral type was obtained by LAMOST. Both spectral types and stellar atmospheric parameters were determined for 5363 EWs. For the other ones, no results were obtained.

3 DISTRIBUTIONS OF STELLAR ATMOSPHERIC PARAMETERS FOR EWS

As aforementioned, the stellar atmospheric parameters of 5363 systems were determined and their relative period distribution is the same as that of all EWs in VSX. Therefore, they could be used to investigate the properties of all EWs. During the analyses, when the EWs were observed two times or more, the stellar atmospheric parameters, effective temperature $T_{\rm eff}$, gravitational acceleration $\log(g)$ and metallicity [Fe/H] were averaged and we used the mean values. For RV $V_{\rm r}$, we did not average them because they were observed at different phases and vary with time.

The binary temperature distribution is shown in Figure 3 and the distribution has a main peak near 5700 K (the solid line). This peak corresponds to the temperature of a G3-type main-sequence star with a stellar mass of about 0.97 $M_{\odot}$ (Cox 2000). This indicates that the majority of EWs are solar-type stars that have the proton-proton (p-p) chain nuclear reaction occurring in their cores.

Figure 3 also shows that there is a small peak near 6600 K (the dashed line). This corresponds to the temperature of an F6-type main-sequence star with a stellar mass of about 1.35 $M_{\odot}$. The transition from the first peak to the second small peak may reflect the central nuclear reaction changing from the p-p chain to the carbon-nitrogen-oxygen (CNO) cycle. The distribution of gravitational acceleration $\log(g)$ is plotted in Figure 4. The distribution peaks near 4.16. It is apparent that the sample of EW systems is homogeneous and most EWs are main-sequence binaries. This is in agreement with the idea that EWs are formed from detached main-sequence binaries via the combination of Case A mass transfer and angular momentum loss via magnetic braking (e.g., Qian et al. 2013a).

The metallicity ([Fe/H]) distribution is shown in Figure 5. EW-type binaries are usually composed of two solar-type stars. It is expected that their metallicities are similar to those detected among stars in the solar neighborhood (e.g., Rucinski et al. 2013). However, as visible in Figure 5, the metallicities of 80.6% of EWs are lower than that of the Sun, i.e., $[{\rm Fe/H}] < 0$. For stars in the Galaxy, stellar metallicities are weakly correlated with their ages (e.g., Reid et al. 2007; Feltzing & Bensby 2009). The low metallicities indicate that most EWs are old stellar populations with longer ages. For a few percent of EWs, their metallicities are higher than 0.3 ($[{\rm Fe/H}] > 0.3$). The possibility of unusually high metallicities may be through contamination by material from unseen degenerate objects (e.g., neutron stars or black holes) that are orbiting the binaries. Their progenitors were originally much more massive third stars in triple systems. Ten EWs that have the highest metallicities are shown in Table 4. They are a good source to search for potential degenerate objects (e.g., neutron stars or black holes) orbiting EWs.

The distribution of RV ($V_{\rm r}$) for these EWs is displayed in Figure 6. 7382 RVs for 5363 EWs are used for constructing the figure. A peak is near $V_{\rm r} = -20\,{\rm km\,s^{-1}}$ and the distribution is symmetric. This may reveal that the V_0 of most EWs is close to this value. The amplitudes of RV curves for EWs are about 150–300 $\rm km\,s^{-1}$ (e.g., Rucinski et al. 2001). Figure 6 reflects a statistically random sampling of RV curves for EWs. Sixteen EWs with RVs larger than 200 $\rm km\,s^{-1}$ are shown in Table 5. They may be observed near the maxima or minima of the RV curves of those EWs.

4 STATISTICAL CORRELATIONS BETWEEN ORBITAL PERIOD AND STELLAR ATMOSPHERIC PARAMETERS

The correlations between orbital period and effective temperature $T_{\rm eff}$, gravitational acceleration $\log(g)$ and metallicity [Fe/H] are shown in Figures 7–9, in which 55 EWs with orbital periods longer than 2 d are not displayed in the figures. Their orbital periods are from 2 d to 24 d. Six EWs are also not included in these figures because their orbital periods are unknown. Their atmospheric parameters are listed in Table 6. As shown in the three figures, the vast majority of EWs have periods in the range $0.2 < P < 0.6$ d. The binary components in these short-period systems are usually main-sequence stars. However, there are some EW-type contact binaries with periods over 1 d. As plotted in Figure 8, the gravitational acceleration ($\log(g)$) is weakly correlated with orbital period. The longer the orbital period is, the lower the gravitational acceleration will be. The lower $\log(g)$ of long-period systems indicates that the component stars have evolved from the zero-age main sequence.

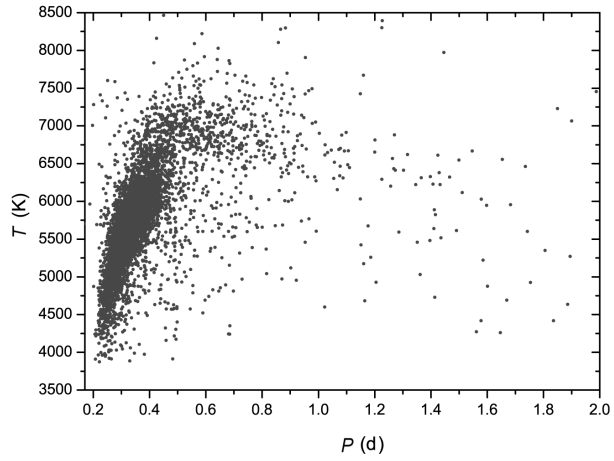

Fig. 7 Correlation between orbital period and effective temperature for EWs observed by LAMOST. 55 EWs with orbital period longer than 2 d are not shown in the figure.

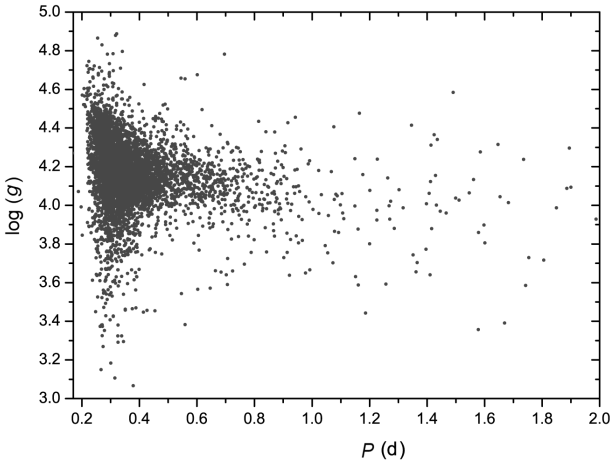

Fig. 8 The same as Fig. 7 but for the correlation between orbital period and gravitational acceleration.

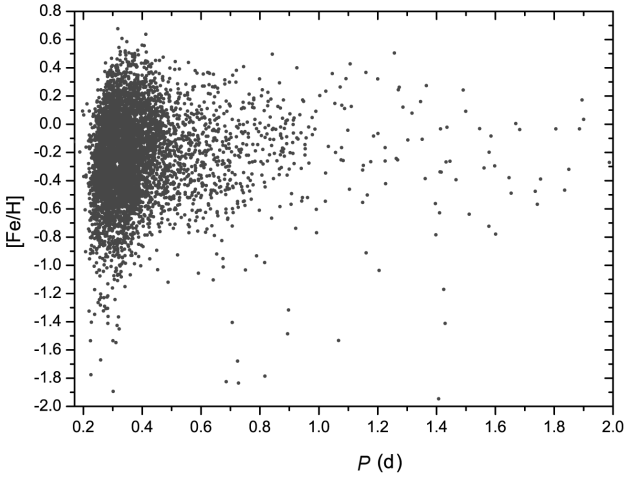

Fig. 9 The same as Fig. 7 and 8 but for the correlation between orbital period and metallicity.

Table 3 Spectral Types Determined by LAMOST (the first 20 observations)

Name	R.A.	Dec.	Type	Period (d)	Distance	Date	Sp.
MS And	022546.86	+395845.5	EW	0.777900	0.559	2013–11–12	K3
GS Aqr	222733.63	–005757.6	EW	0.374067	0.479	2012–10–29	A5V
MR Aur	055133.68	+310652.0	EW	0.690301	1.541	2011–11–10	A2IV
MR Aur	055133.68	+310652.0	EW	0.690301	1.541	2011–12–25	A1V
CK Boo	143503.76	+090649.4	EW/RS	0.355152	0.093	2016–04–24	F0
GH Boo	141451.51	+273415.7	EW	0.65951	0.833	2015–01–15	A8III
GH Boo	141451.51	+273415.7	EW	0.65951	0.053	2016–05–15	G7
GQ Boo	145936.67	+250244.9	EW	0.3846402	0.126	2012–06–05	G8
GW Cnc	084812.69	+210713.8	EW	0.281413	0.053	2015–03–08	G7
UZ CMi	075051.76	+033903.5	EW/DW	0.551361	0.180	2013–01–23	F6
BB CMi	075124.55	+045439.2	EW	0.792866160	0.204	2013–01–23	F0
SS Com	124939.08	+184211.9	EW/KW	0.412822	0.076	2016–05–19	G7
EY Com	131355.38	+310454.1	EW/KW	0.2993278	0.715	2012–02–26	K5
LP Com	123305.52	+270803.6	EW	0.33793358	0.107	2012–01–23	K4
LP Com	123305.52	+270803.6	EW	0.33793358	0.107	2012–01–11	K1
V2213 Cyg	192857.89	+430625.5	EW	0.350094	0.220	2014–09–13	G7
V2284 Cyg	192955.02	+485500.1	EW	0.306994	0.014	2013–09–14	G7
V2284 Cyg	192955.02	+485500.1	EW	0.306994	0.004	2015–10–01	G7
IV Dra	153623.26	+531911.3	EW	0.268105	0.017	2013–05–03	K5
IV Dra	153623.26	+531911.3	EW	0.268105	0.201	2012–06–17	K3

Table 4 Ten EWs with the Highest Metallicities

Name	Period (d)	Sp.	T (K)	$\log(g)$	[Fe/H]	$V_{\rm r}$ (km s^{-1})
CSS_J080956.0+131054	0.316903	K1	5692.04	4.491	0.677	–50.76
VSX J001137.3+303145	0.41222	F9	5719.4	4.088	0.637	–66.27
CSS_J083051.6+185801	0.331662	G5	5323.88	4.104	0.609	15.62
NSVS 2729390	0.347679	K0	5490.45	4.36	0.586	–63.81
ASAS J163229+0818.1	0.399559	G8	5815.14	4.254	0.56	–12.5
NSVS 4231740	0.40694612	F9/G5	5809.96	4.085	0.557	35.28
V1047 Her	0.32073733	K1	5466.2	4.211	0.545	–85.15
CSS_J032658.1+142940	0.385214	G7	5650.16	4.336	0.524	–2.23
CSS_J072417.0+224103	0.342338	G8/K1	5497.9	4.233	0.519	–37.3
CSS_J002629.5+445324	0.325968	K1/K3	5043.48	4.398	0.514	–0.99

Figure 7 shows that there is a good correlation between the orbital period and effective temperature $T_{\rm eff}$ for short-period EWs (e.g., $P < 0.6$ d). This is more clearly seen in Figure 10 where only short-period EWs are shown. The red dashed line in Figure 10 refers to the peak value of the period distribution. The relation is similar to the period-color relation for EWs (e.g., Eggen 1961, 1967; Rucinski 1998; Terrell et al. 2012). Both main-sequence components in short-period EWs fill their critical Roche lobes and undergo CCE. It is expected that longer-period systems should have higher-mass components with higher temperatures (e.g., Qian 2003). However, this relation shows a large scatter. This may be caused by the effect of the presence of third stars. Two examples of this case are 1SWASP J193127.17+465809.1 and 1SWASP J235935.22+362001.5 (e.g., Lohr et al. 2013). They are extremely short-period EWs with orbital periods 0.1976295 and 0.2016714 d respectively. It is expected that they should be extremely cool binary systems. However, their spectral types determined by LAMOST are F0 with temperatures of 7027 K and 7294 K respectively. The possibility of a third body being present with spectral type of F0 can cause this difference. New spectroscopic and photometric data are very useful for studying these two interesting systems. Their positions in Figure 10 are shown as magenta solid triangles that greatly deviate from the general trend.

The other possible cause for the large scatter in the period-temperature relation is that the peri-

Table 5 EWs Observed by LAMOST with RVs Larger than 200 km s^{-1}

Name	Period (d)	Sp.	T (K)	$\log(g)$	[Fe/H]	$V_{\rm r}$ (km s^{-1})
UY Hya	0.7275	A2V	6697.05	4.233	–1.834	359.43
CSS_J212703.2+100332	0.452204	A5V	7065.8	4.27	–1.022	–321.77
CSS_J212703.2+100332	0.452204	A3V	6817.47	4.248	–1.039	–316.4
CSS_J005447.7+284030	0.314908	F0	6737.72	4.265	–0.888	–306.44
CSS_J032645.2+004931	0.705836	F5	5826.79	4.062	–1.405	–304.7
CSS_J112812.6+045202	0.316715	F5	5985.71	3.965	–0.881	301.29
CSS_J214828.6+090336	1.42465	F0	6611.71	4.365	–1.17	–285.31
CSS_J010448.7+373231	0.283694	F0	6139.34	4.047	–1.411	–276.72
CSS_J014525.5+360334	0.270282	G7	5342.15	4.101	–0.579	–264.58
CSS_J170410.6+274628	0.709314	A9V	6711.52	4.136	–0.627	–255.78
NSVS 7285749	0.323629	F0	6438	4.322	–1.018	242.96
CSS_J115356.5–022540	0.224256	K2	5074.82	4.745	–0.917	240.42
CSS_J072136.0+403327	0.340065	F4	6714.6	4.409	0.467	230.7
NSVS 7285749	0.323629	F0	6477.27	4.323	–0.963	222.12
CSS_J012955.1+391130	0.317905	F7	5932.42	4.1	–0.52	–216.98
LINEAR 14668373	0.224377	G8	4989.28	4.014	–1.591	–212.1
CSS_J032034.5+203607	0.320948	K5	5874.96	4.888	0.005	210.36

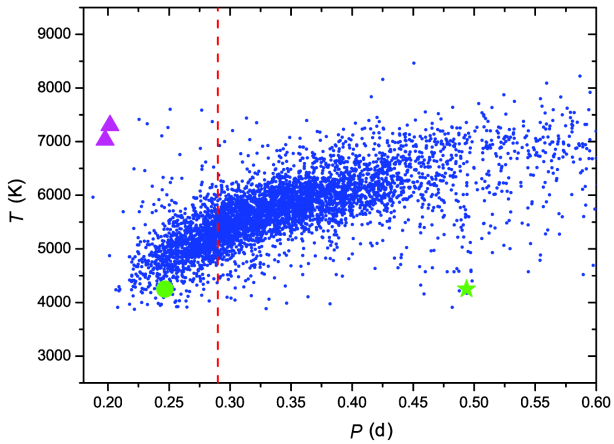

Fig. 10 Correlation between the orbital period and effective temperature for EWs with orbital periods shorter than 0.6 d. Magenta solid triangles refer to the positions of 1SWASP J193127.17+465809.1 and 1SWASP J235935.22+362001.5 that may contain bright third bodies. The green solid star represents the position of CSS_J080814.1+184933 with an inaccurate period, while the green solid circle to the left signifies the revised one.

ods of some binaries are inaccurate. One example is CSS_J080814.1+184933. Its orbital period given in VSX is 0.493868 d. The green solid star in Figure 10 refers to its position which does not follow the general trend of the period-temperature relation. The phased light curve from using this period is shown in Figure 11. As we see in the figure, there are two primary minima and two secondary minima in one phased light curve. This indicates that the period is inaccurate. By using those new data, the period of the binary was revised to 0.246746 d. The phased light curve with the revised period is displayed in Figure 12 which is a typical EW-type light curve. The green solid circle in Figure 10 represents the updated position of the binary with the revised period. As shown in Figure 10, the period-temperature relation is tight, but this relation is not linear.

Relations between the orbital period and $\log(g)$ and [Fe/H] for short-period EWs are shown in Figures 13 and 14 respectively. The positions of the three special EWs are also plotted in the two figures. Like what is depicted in Figure 10, the dashed lines represent the peak value of the period distribution. Figure 13 shows that

Table 6 LAMOST Observations of EWs without Orbital Periods

Name	R.A. (deg)	Dec. (deg)	Date	Sp.	T (K)	$\log(g)$	[Fe/H]	$V_{\rm r}$ (km s^{-1})
V0674 Per	54.115	36.37417	2014–11–13	K0	5046.24	4.307	–0.162	–39.99
V0726 Aur	80.69046	29.11806	2014–11–03	F9				
NSV 3633	113.47608	48.00353	2013–11–22	F5	6327.91	4.174	–0.428	1.75
NSV 3633	113.47608	48.00353	2015–01–31	F5	6370.36	4.121	–0.348	4.84
NSV 3633	113.47608	48.00353	2016–02–19	F5	6353.80	4.128	–0.362	14.10
NSV 5580	185.6305	25.82833	2012–01–11	F7	6277.52	4.312	0.051	1.75
NSV 5580	185.6305	25.82833	2012–02–01	F7	6230.28	4.341	0.033	–17.33
NSV 5652	187.37508	29.51272	2012–01–11	F7	6227.60	4.121	0.063	–30.58
MG1 809127	240.96542	2.92944	2016–05–10	A5V				
Konkoly V14	81.62869	12.95734	2013–10–02	F0	6857.67	3.474	0.396	–16.07
SvkV34	85.75447	40.95046	2012–02–18	K5	4520.01	4.382	–0.001	23.93

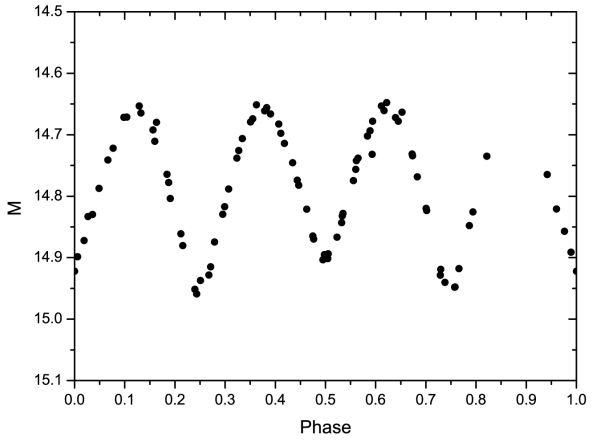

Fig. 11 Phased light curve of CSS_J080814.1+184933 by using the orbital period (0.493868 d) given in VSX.

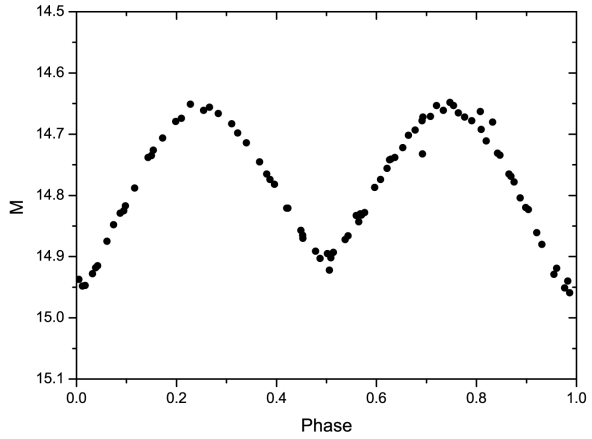

Fig. 12 The light curve of CSS_J080814.1+184933. The phases were computed with the revised period 0.246746 d.

$\log(g)$ is weakly correlated with orbital period. The relation for short-period systems ($P < 0.29$ d) is deeper than that for long-period ones ($P > 0.29$ d). As displayed in Figure 14, most of the EWs have lower metallicities (below the red solid line). The metallicity is also weakly correlated with orbital period. Short-period EWs, with period shorter than 0.25 d, have metallicities below zero.

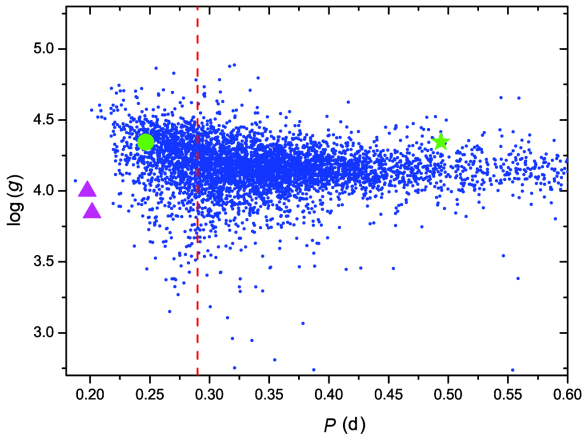

Fig. 13 The relation between orbital period (P) and gravitational acceleration $\log(g)$ for short-period EWs. Symbols are the same as those in Fig. 10.

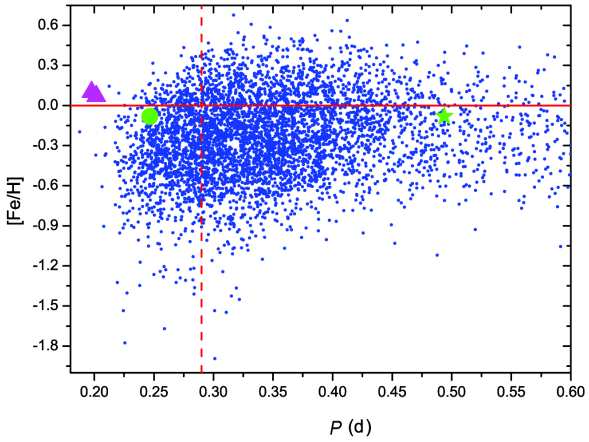

Fig. 14 The relation between orbital period (P) and metallicity [Fe/H] for short-period EWs. Symbols are the same as those in Figs. 10 and 13.

5 DISCUSSION AND CONCLUSIONS

Numerous EWs have been discovered through several large photometric surveys (e.g., CSS, the asteroid survey LINEAR, ASAS and NSVS). However, spectroscopic data are lacking for those EWs. Among 40 785 EWs listed in the VSX catalog, 7938 were observed in the LAMOST spectral survey from 2011 October 24 to 2016 November 30. We catalog those EWs and their spectral types are given. We also present stellar atmospheric parameters for 5363 of them. By analyzing 25 EWs observed five times or more by LAMOST, we show that the standard errors of the effective temperatures, gravitational acceleration and metallicity are usually lower than 110 K, 0.19 dex and 0.11 dex, respectively. These results may indicate that the spectra of EWs have sufficient tracers necessary for unique determination of atmospheric parameters and the extracted parameters could reach the mentioned level of precision. However, to check the results obtained by LAMOST, a careful selection and a detailed spectroscopic investigation of some EWs observed by LAMOST are needed. We are observing some EWs spectroscopically and will determine their stellar atmospheric parameters and compare them with those obtained by LAMOST.

The derived effective temperatures as well as the spectral types by LAMOST are very useful for generating the photometric solutions of their light curves. The other atmospheric parameters provide us with valuable information to understand the formation and evolution-

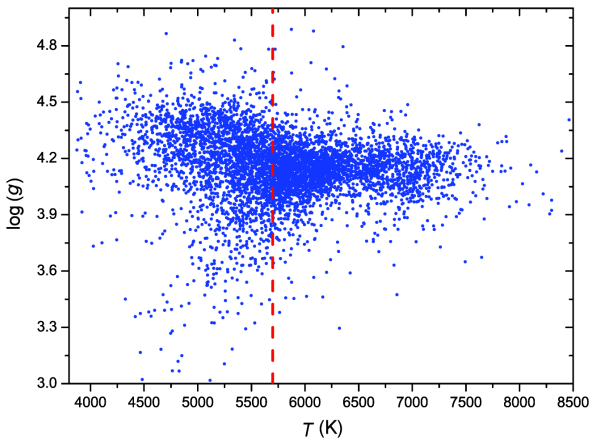

Fig. 15 The relation between effective temperature (T) and gravitational acceleration $\log(g)$ for EWs. The red dashed line represents the peak of the temperature distribution at 5700 K.

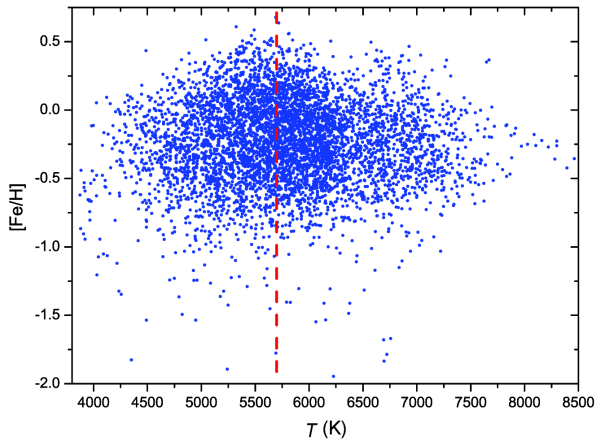

Fig. 16 The relation between effective temperature (T) and metallicity [Fe/H] for EWs. The red dashed line represents the peak of the temperature distribution.

ary state of EWs. We found that the peak of the period distribution is near 0.29 d, which is shorter than that given by previous investigators (e.g., Paczyński et al. 2006). This indicates that a large number of short-period faint EWs were discovered recently with deep photometric surveys. The distributions of effective temperature (T), gravitational acceleration ($\log(g)$), metallicity ([Fe/H]) and RV are presented for observed EWs. There are two peaks in the temperature distribution that correspond to p-p chain and CNO nuclear reactions respectively in the cores of the components. The distribution of gravitational acceleration $\log(g)$ indicates that the components of most EWs are main-sequence stars, which is consistent with the idea that EWs are formed from detached main-sequence binaries via a combination of Case A mass transfer and angular momentum loss via magnetic braking (e.g., Qian et al. 2013b).

The detected metallicities of most sample stars (about 80.6%) are below zero. Since stellar metallicities are weakly correlated with their ages (e.g., Reid et al. 2007; Feltzing & Bensby 2009), this detection reveals that EW-type systems are old stellar populations. This supports the assumption that EWs need a long-term pre-contact evolution with timescales from a few hundred million to a few billion years. A few percent of EWs with unusually high metallicities may be contaminated by material from the evolutionary processes of unseen neutron stars or black holes in the systems. The progenitors of these unseen degenerate objects were originally much more massive third stars in triple systems. To date, neutron stars and black holes have usually been discovered

in X-ray binaries through their X-ray radiation. They are formed through common envelope evolution and are influenced by their companion stars. If these unseen degenerate objects are confirmed, they will represent a new population of neutron stars and black holes (e.g., Qian et al. 2008; Ziolkowski 2010).

The correlations between orbital period and effective temperature, gravitational acceleration and metallicity are shown in previous sections. The scatters of those figures may be mainly caused by the presence of third bodies. EWs have the shortest period and lowest angular momentum among main-sequence binaries. It is assumed that they have a third body that plays an important role in their formation by removing angular momentum from the central binary (e.g., Qian et al. 2006, 2007, 2013a; Zhu et al. 2013b) For some systems, their orbital periods are inaccurate, which also causes scatters in those diagrams. It is shown that the relation between orbital period and effective temperature is tight but not linear.

Both gravitational acceleration and metallicity are weakly correlated with orbital period. The metallicities of all short-period EWs, with period shorter than 0.25 d, are below zero. These indicate that the physical properties of EWs mainly depend on their orbital periods. The formations and evolutionary states of EWs with different orbital periods may be quite different. This conclusion is supported by the relations between effective temperature (T) and gravitational acceleration $\log(g)$ and metallicity [Fe/H], which are shown in Figures 15 and 16 respectively. The dashed lines in the two figures refer to the peak of the temperature distribution at 5700 K. It is found that both gravitational acceleration and metallicity are weakly correlated with effective temperature. Those extremely short-period EWs ($P < 0.29$ d; $T < 5700$ K) usually have higher gravitational acceleration $\log(g)$ and lower metallicity [Fe/H]. They are main-sequence stars with little evolution and are older than their hotter cousins that have longer periods. This may suggest that they have a long timescale of pre-contact evolution and their formation and evolution are mainly driven by angular momentum loss via magnetic braking.

Acknowledgements This work is partly supported by the National Natural Science Foundation of China (No. 11325315). The Guo Shou Jing Telescope (the Large Sky Area Multi-Object Fiber Spectroscopic Telescope, LAMOST) is a National Major Scientific Project built by the Chinese Academy of Sciences. Funding for the project has been provided by the National Development and Reform Commission. LAMOST is operated and managed by National Astronomical Observatories, Chinese Academy of Sciences. Spectroscopic observations used in the paper were obtained with LAMOST from 2011 October 24 to 2016 November 30.

References

Becker, A. C., Bochanski, J. J., Hawley, S. L., et al. 2011, ApJ, 731, 17

Bradstreet, D. H., & Guinan, E. F. 1994, in Astronomical Society of the Pacific Conference Series, 56, Interacting Binary Stars, ed. A. W. Shafter, 228

Cox, A. N. 2000, Introduction, ed. A. N. Cox, Allen's Astrophysical Quantities, ed. A. N. Cox (New York: AIP Press; Springer), 1

Cui, X.-Q., Zhao, Y.-H., Chu, Y.-Q., et al. 2012, RAA (Research in Astronomy and Astrophysics), 12, 1197

Drake, A. J., Djorgovski, S. G., Mahabal, A., et al. 2009, ApJ, 696, 870

Drake, A. J., Graham, M. J., Djorgovski, S. G., et al. 2014, ApJS, 213, 9

Eggen O. J., 1961, Royal Obs. Bull., 31

Eggen, O. J. 1967, MmRAS, 70, 111

Feltzing, S., & Bensby, T. 2009, in IAU Symposium, 258, The Ages of Stars, ed. E. E. Mamajek, D. R. Soderblom, & R. F. G. Wyse, 23

Gao, H., Zhang, H.-W., Xiang, M.-S., et al. 2015, RAA (Research in Astronomy and Astrophysics), 15, 2204

Guinan, E. F., & Bradstreet, D. H. 1988, in NATO Advanced Science Institutes (ASI) Series C, 241, eds. A. K. Dupree & M. T. V. T. Lago, 345

Kaluzny, J., & Rucinski, S. M. 1993, in Astronomical Society of the Pacific Conference Series, 53, Blue Stragglers, ed. R. A. Saffer, 164

Koleva, M., Prugniel, P., Bouchard, A., & Wu, Y. 2009, A&A, 501, 1269

Lohr, M. E., Norton, A. J., Kolb, U. C., et al. 2013, A&A, 549, A86

Luo, A.-L., Zhang, H.-T., Zhao, Y.-H., et al. 2012, RAA (Research in Astronomy and Astrophysics), 12, 1243

Luo, A.-L., Zhao, Y.-H., Zhao, G., et al. 2015, RAA (Research in Astronomy and Astrophysics), 15, 1095

Paczyński, B., Szczygieł, D. M., Pilecki, B., & Pojmański, G. 2006, MNRAS, 368, 1311

Palaversa, L., Ivezić, Ž., Eyer, L., et al. 2013, AJ, 146, 101

Pojmanski, G. 1997, Acta Astronomica, 47, 467

Pojmanski, G., Pilecki, B., & Szczygiel, D. 2005, Acta Astronomica, 55, 275

Prugniel, P., & Soubiran, C. 2001, A&A, 369, 1048

Prugniel, P., Soubiran, C., Koleva, M., & Le Borgne, D. 2007, astro-ph/0703658
Qian, S. 2003, MNRAS, 342, 1260
Qian, S.-B., Liao, W.-P., & Fernández Lajús, E. 2008, ApJ, 687, 466
Qian, S.-B., Liu, L., & Kreiner, J. M. 2006, New Astron., 12, 117
Qian, S.-B., Xiang, F.-Y., Zhu, L.-Y., et al. 2007, AJ, 133, 357
Qian, S.-B., Zhang, J., Wang, J.-J., et al. 2013a, ApJS, 207, 22
Qian, S.-B., Liu, N.-P., Li, K., et al. 2013b, ApJS, 209, 13
Qian, S.-B., Wang, J.-J., Zhu, L.-Y., et al. 2014, ApJS, 212, 4
Reid, I. N., Turner, E. L., Turnbull, M. C., Mountain, M., & Valenti, J. A. 2007, ApJ, 665, 767
Rucinski, S. M. 1998, AJ, 116, 2998
Rucinski, S. M., Lu, W., Mochnacki, S. W., Ogłoza, W., & Stachowski, G. 2001, AJ, 122, 1974
Rucinski, S. M., Pribulla, T., & Budaj, J. 2013, AJ, 146, 70
Samus, N. N., Kazarovets, E. V., Durlevich, O. V., Kireeva, N. N., & Pastukhova, E. N. 2017, Astronomy Reports, 61, 80
Terrell, D., Gross, J., & Cooney, W. R. 2012, AJ, 143, 99
Wang, S.-G., Su, D.-Q., Chu, Y.-Q., Cui, X., & Wang, Y.-N. 1996, Appl. Opt., 35, 5155
Watson, C. L. 2006, Society for Astronomical Sciences Annual Symposium, 25, 47
Woźniak, P. R., Vestrand, W. T., Akerlof, C. W., et al. 2004, AJ, 127, 2436
Wu, Y., Singh, H. P., Prugniel, P., Gupta, R., & Koleva, M. 2011a, A&A, 525, A71
Wu, Y., Luo, A.-L., Li, H.-N., et al. 2011b, RAA (Research in Astronomy and Astrophysics), 11, 924
Wu, Y., Du, B., Luo, A., Zhao, Y., & Yuan, H. 2014, in IAU Symposium, 306, Statistical Challenges in 21st Century Cosmology, eds. A. Heavens, J.-L. Starck, & A. Krone-Martins, 340
Zhao, G., Zhao, Y.-H., Chu, Y.-Q., Jing, Y.-P., & Deng, L.-C. 2012, RAA (Research in Astronomy and Astrophysics), 12, 723
Zhu, L. Y., Qian, S. B., Liu, N. P., Liu, L., & Jiang, L. Q. 2013a, AJ, 145, 39
Zhu, L.-Y., Qian, S.-B., Zhou, X., et al. 2013b, AJ, 146, 28
Zhu, L.-Y., Zhao, E.-G., Zhou, X., 2016, RAA (Research in Astronomy and Astrophysics), 16, 68
Ziolkowski, J. 2010, Mem. Soc. Astron. Italiana, 81, 294